Improvement of Laser Electromagnetic Hybrid Thruster

IEPC-2013-265

Presented at the 33rd International Electric Propulsion Conference,
The George Washington University • Washington, D.C. • USA
October 6 – 10, 2013

Yuji Oigawa[1] and Hideyuki Horisawa[2]
Tokai University, Kitakaname, Hiratsuka City, Kanagawa, 259-1292

Ikkoh Funaki[3]
Japan Aerospace Exploration Agency, Sagamihara, Kanagawa, 229-8510, Japan

Abstract: An objective of this study was to observe the plasma acceleration process and to understand the mechanism of high speed plasma generation. To observe the plasma behaviors between the rectangular electrodes of the Laser-Electromagnetic Hybrid Thruster, an ICCD camera was utilized. From the time-resolved images, behaviors of the plasma wavefront were analyzed and speeds of the plasma were estimated. Moreover, measurement of impulse bit and Time-of flight (TOF) measurement were also conducted.

Nomenclature

V_c	=	charge voltage in capacitor
E_c	=	charge energy in capacitor
v_p	=	speed of plasma
t_d	=	delay time from laser ablation
I_{sp}	=	specific impulse
η_{th}	=	thrust efficiency

I. Introduction

The current trend towards small spacecraft, which is not only mass limited but also power limited, has produced a strong interest in development of micropropulsion devices.[1-4] The significance in reducing launch in the past, many very small spacecraft has lacked propulsion systems altogether, future micro-spacecraft will require significant propulsion capability in order to provide a high degree of maneuverability and capability. The benefit of using electric propulsion for the reduction of spacecraft mass will likely be even more significant for mass limited micro-spacecraft missions.[2-4] Feasibility studies of micro-spacecraft are currently under development for a mass less than 100 kg with an available power level for propulsion of less than 100 watts.[2-4] Various potential propulsion systems for micro-spacecraft applications, such as ion thrusters, field emission thrusters, pulsed plasma thrusters (PPTs), vaporizing liquid thrusters, resistjets, microwave arcjets, pulsed arcjets, etc., have been proposed and are under significant development for primary and attitude control applications.[4] In particular, the PPTs are expected to be used for microsatellites and their long term missions because of the precise impulse bit controllability.

On the other hand, small-sized onboard laser plasma thrusters are also under significant development with rapid evolutions of novel compact laser systems. One of the advantages of laser thrusters is that they can induce high specific impulse. In addition, the system can be very simple and small with significant controllability of the thrust.[5-8] In order

[1] Graduate student, Department of Aeronautics and Astronautics, yuji.oigawa@gmail.com.
[2] Professor, Department of Aeronautics and Astronautics, horisawa@keyaki.cc.u-tokai.ac.jp.
[3] Associate Professor, Institute of Space and Astronautical Science, funaki@isas.jaxa.jp.

to improve thrust performances and system simplicities of those conventional electric and laser propulsion systems, a preliminary study on a laser-electric hybrid acceleration system have been conducted by the authors.[9-14]

II. Laser-Electromagnetic Hybrid Thruster

A schematic of the rectangular Laser-Electromagnetic Hybrid Thruster (L-EM thruster) is illustrated in Fig. 1.[9-14] It utilizes laser-beam irradiation to induce plasma ionized from a solid propellant between the anode and cathode is increased, the plasma can be heated and further ionized through joule heating. Thus, the electrothermal acceleration effect becomes significant. When a current exceeds more than one thousand amperes, an electromagnetic acceleration effect becomes significant. With interaction of the current and self-induced magnetic field, a streamwise acceleration is provided.[18, 20]

A basic idea of these systems is that a bunch of laser-ablation plasma, induced through laser irradiation on a solid target, is additionally accelerated by electrical means. Since any solid material can be used for the propellant in these cases, no tanks, no valves, or piping systems are required for the propulsion system. Also, various materials in any phase can be used for the propellant. Therefore, the system employing this technique can be simple and compact. As the laser-ablation plasma has a directed initial speed of tens of km/s, which will be further accelerated by electrical means, significantly high specific impulses can be expected.

In the above hybrid cases, depending on different factors such as electrode configuration, plasma density, electrical input-power (voltage and current), etc., acceleration mechanisms for the laser-ablation plasma can be varied into three types, i.e., 1) electrostatic acceleration, 2) electromagnetic acceleration, and 3) electrothermal acceleration as shown in Figure.2, although 2) usually occurs simultaneously with 3). Especially for the laser-ablation plasma, depending on laser conditions such as pulse energy, fluence, etc., plasma density distribution can be widely controlled. Moreover, this can also be increased through additional electric discharges. Properly controlling a power source, or voltage and current, with optimized electrode configuration for additional electric acceleration, each acceleration mechanism can be adopted. Because the use of a shorter laser pulse enables a shorter pulsed-plasma generation, a significantly high peak current can be induced. Since the force induced in the accelerator is dependent on the square of the current, significant improvements in acceleration characteristics can be expected. In addition, depending on laser power, laser-induced plasma produced from a solid propellant usually has a directed initial speed, and this can also contribute to an improvement in the acceleration performance.

Therefore, propulsion system that is able to satisfy all the above acceleration schemes through 1) to 3) will be achieved with one thruster configuration. Namely this system enables a robust conversion between high specific impulse operation and high thrust density operation in regard to mission requirements as shown Fig. 2. Each of two typical accelerators, a laser-electrostatic hybrid accelerator and a laser-electromagnetic hybrid accelerator, is currently under investigation.

III. Research Motivation

Variations of specific impulse with discharge energy are plotted in Fig. 3 for various acceleration channel configurations. From the figure, it can be seen in all the cases that specific impulse increased with the increase of the charging energy. Moreover, thrusters with longer channel length showed higher specific impulses. The highest specific impulse of 7,200 sec was obtained with the 10 mm x 50 mm thruster at the highest charging energy of 8.6 J.[17]

However, mechanism of generation of high specific impulse, or namely high speed plasmas, is still unknown.

Therefore, an objective of this study is to observe the plasma acceleration process and to understand the mechanism of high speed plasma generation. To observe the plasma behaviors between the rectangular electrodes of the L-EM thruster, an ICCD camera was utilized. From the time-resolved images, behaviors of the plasma wavefront were analyzed and speeds of the plasma were estimated. Moreover, to estimate the speed of fast ions, time-of flight (TOF) measurement was conducted. In addition, to evaluate the thrust performance, impulse bit measurement and mass shot measurement were also conducted.

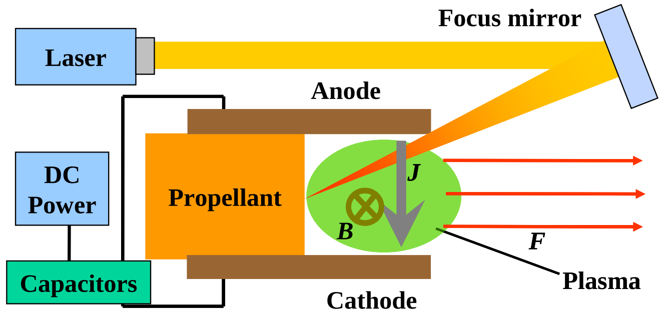

Figure 1. Schematic of illustration of a rectangular laser-electromagnetic hybrid thruster (L-EM thruster).

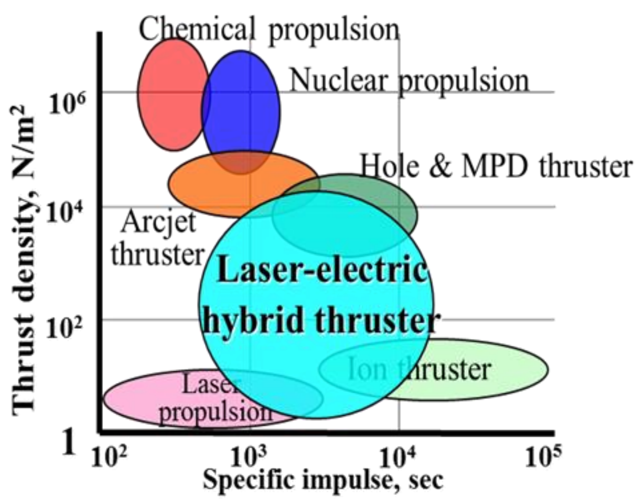

Figure 2. Classification of laser-hybrid propulsion systems based on energy contributions, such as pure laser propulsion mode, electric assisted laser propulsion (LP) mode, hybrid propulsion mode, laser-assisted electric propulsion (EP) mode, and pure electric propulsion mode.

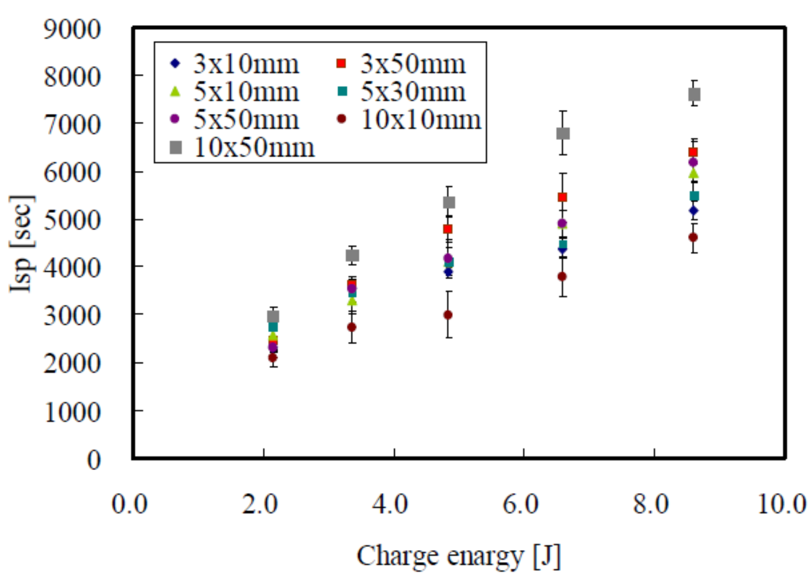

Figure 3. Variation of specific impulse with charge energy for thrusters with various electrode geometries (electrode length × electrode height).[17]

IV. Experimental setup

A. Plasma Behavior Analysis

1. Plasma Plume Observation with ICCD camera

To observe the plasma behaviors between the rectangular electrodes of the L-EM thruster, the time-resolved imaging with an ICCD camera was conducted. From the time-resolved images, behaviors of the plasma wavefront were analyzed and speeds of the plasmas were estimated.

A photo of the thruster is shown in Fig. 4, in which electrodes made of molybdenum and propellant and insulator made of alumina ceramics. Configuration of the thruster is listed in Table 1.

A schematic of experimental set up for ICCD camera observation is shown in Fig. 5. The LA-PPT is placed in vacuum chamber (2.7×10^{-3} Pa) and ignited through a laser ablation plasma induced with a focused laser pulse at a center surface of the propellant. As for the laser oscillator, an Nd:YAG laser (CONTINUUM INC., Surelite II, wave length: 1,064 nm, pulse width 5 ns, pulse energy: 400 mJ) was utilized. A time-resolved image can be monitored with an ICCD camera (ANDOR TECHNOLOGY, minimum gate width: 2 ns).

Generating an arbitrary delay with a delay generator triggered by a Q-switch output signal of the laser, the ICCD camera was synchronized with a laser pulse. Since the phenomena were highly reproducible, it was possible to obtain images of temporal behaviors of plasma formation and acceleration process with 2 ns resolution through changing the delay.

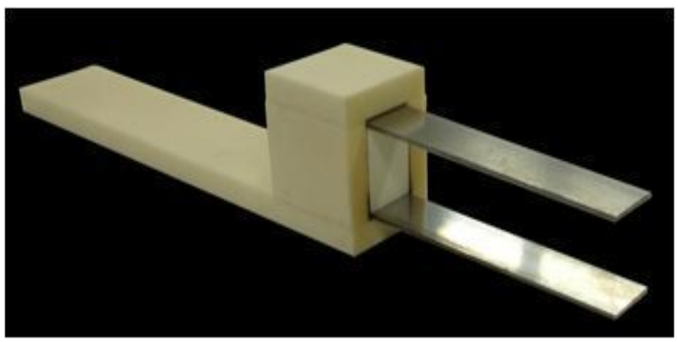

Figure 4. Schematic photo of Laser-Electromagnetic Hybrid Thruster (L-EM thruster).

Table 1. Configuration of L-EM thruster

Channel length: l	50 mm
Channel width: w	10 mm
Channel gap: h	15 mm
Electrode material	Mo
Propellant material	Al_2O_3
Body	Al_2O_3

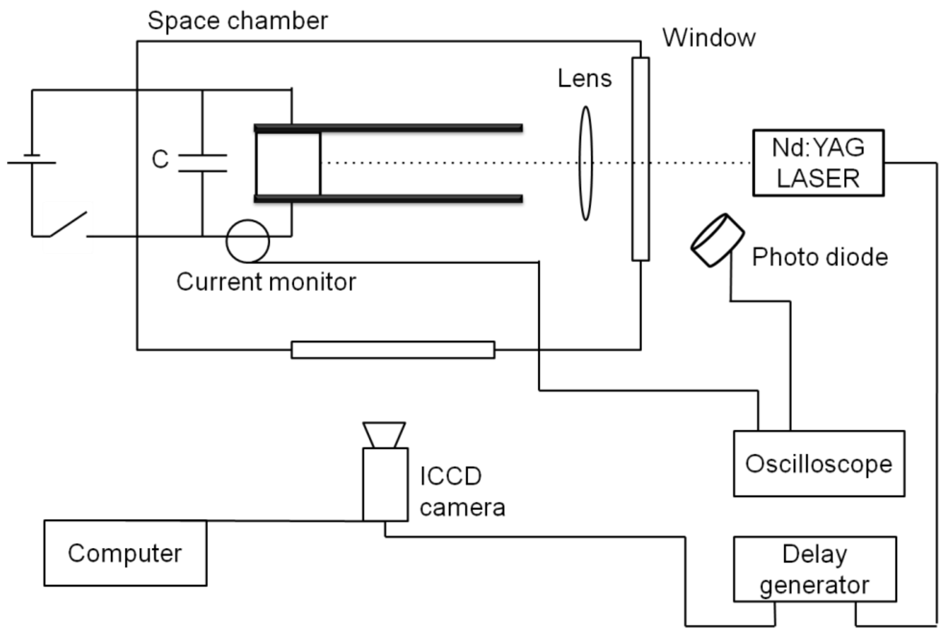

Figure 5. Schematic of experimental setup for ICCD camera observation.

2. Plasma Behavior Analysis

Time-resolved images at various moments were captured by the ICCD camera, and then analyzed with an image processing software. In the analysis, emission intensity distributions of the parallel to a longitudinal direction (x-axis) of the thruster were plotted and evaluated from the image data as shown schematically in Fig. 6. As shown in the figure, motion, or a velocity, of a wavefront (an inflection point of emission distribution) of plasma induced and accelerated in the thruster were extracted. A typical between two images was 100 ns for plasma velocity evaluation.

Since the plasma behaviors are non-uniform across the electrodes, plasma emission distribution and motions were evaluated along three lines (center line (y=0 mm), anode side (y = 3 mm), cathode side (y = -3 mm)) parallel to a longitudinal axis (*x*-axis) of the thruster shown in Fig. 7.

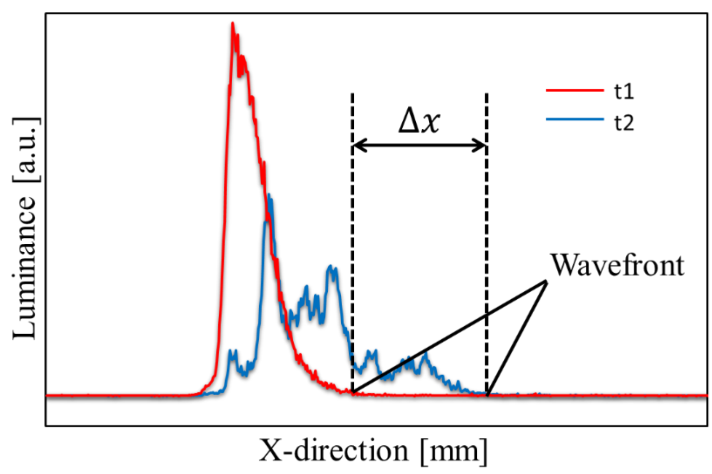

$$v_p = \frac{\Delta x}{\Delta t}$$

Figure 6. Schematic of emission intensity distributions of the plasma parallel to x-axis of the thruster to determine motion of wavefront and velocity of plasma.

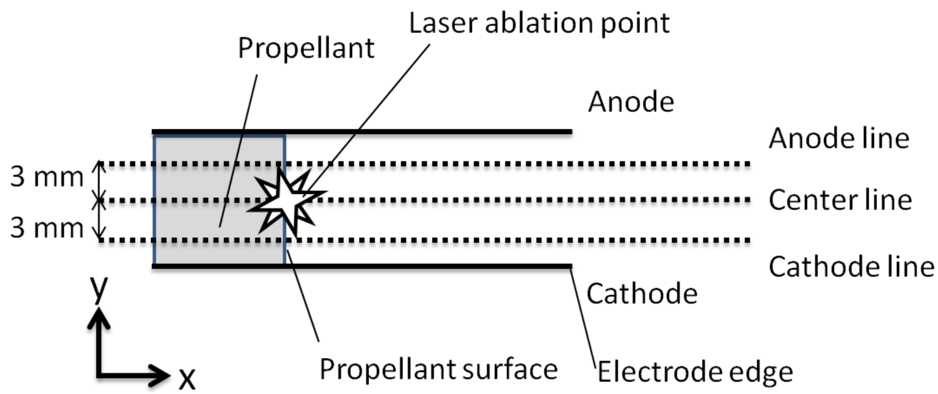

Figure 7. Schematic illustration of three lines (center line(y=0 mm), cathode side (y = -3 mm), and anode side (y = 3 mm)) parallel to a longitudinal axis (x-axis) of the thruster.

B. Time of Flight (TOF) Measurement of Ions with Faraday Cup for Ion Speed Evaluation

A schematic of experimental set up for time of flight measurement with Faraday cup is shown in Fig. 8.

Temporal variation of the ion currents contained in a pulsed plasma plume was monitored with a Faraday cup. The Faraday cup consists of an electron-suppressor grid in front of a collector electrode. A typical distance between the thruster edge and Faraday cup was 400, 600 mm.

Speed of fast ions was estimated with a time when peak ion current was measured and the distance.

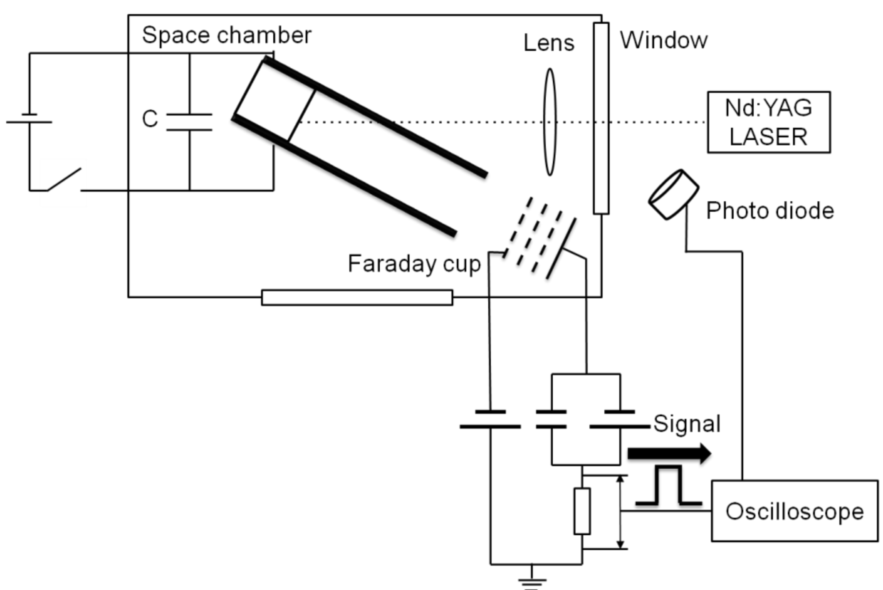

Figure 8. Schematic of time-of-flight measurement of ions with Faraday cup for ion speed evaluation.

C. Evaluation of Thrust Performance

1. Impulse Bit Measurement

To measure an impulse bit of the L-EM thruster, impulse bit measurement by a pendulum type thrust stand was conducted. Figure 9 show a schematic of the impulse bit measurement system. A pendulum type thrust stand was installed in the vacuum chamber. The thrust stand based on a pendulum measures a reaction force exerted on a thruster during operation. A thruster is installed on the thrust stand, and impulse bit is calculated from the response by the reaction force of the thrust. Displacement of the pendulum arm (length: 280 mm) was measured by an inductive displacement sensor (EMIC CORP., NPA-010, resolution: 0.5 μm, range: 0-1.0 mm, output voltage: 0-1.0 V). Wave of output voltage was measured by an oscilloscope (Tektronix, TDS3034B, band width: 300MHz, the best sampling rate: 2.5 GS/s).

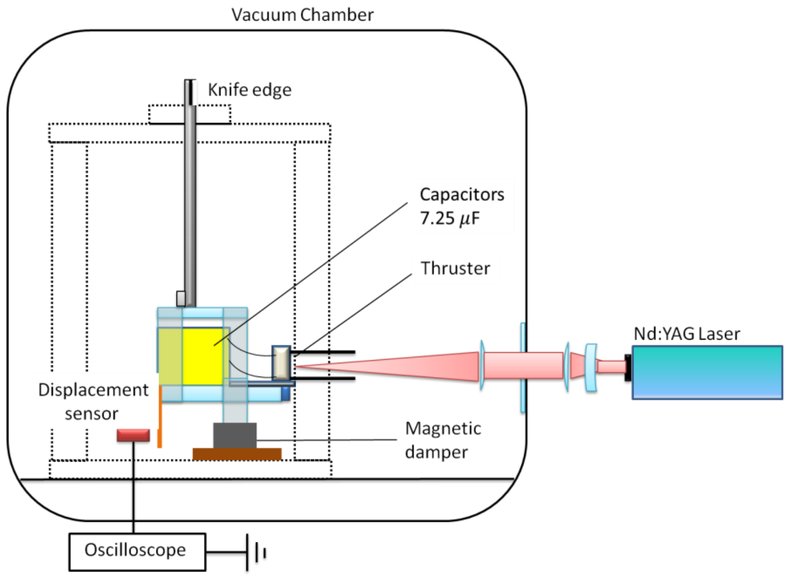

Figure 9. Schematic of impulse bit measurement system.

2. Mass Shot Measurement

For the measurement of a mass-shot per pulse-shot of the propellant, or propellant consumption rate per shot, the measurement of the removed volumes of the propellant target surface after the number of shots were conducted with the vision measuring system (Mitsutoyo, QV-APEX302) because propellant consumption rate is mainly controlled by laser induced plasma.[13] A typical number of pulse-shots to measure the mass-shot was 500 times.

V. Results and Discussion

A. Discharge Current Measurement

Figure 10 shows temporal variations of discharge current waveforms for V_c = 500 V to 2000 V. At 3μs the currents cross zero for all V_cs. At 4.5 μs the currents reach the smallest (negative peak) values, which is -5 kA for V_c = 2000 V. After crossing zero at 6μs, the currents reach the second peak values, which is 2.5 kA for V_c = 2000 V. After reaching the second smallest values at 10.5 μs, the currents converge into zero at 12 μs.

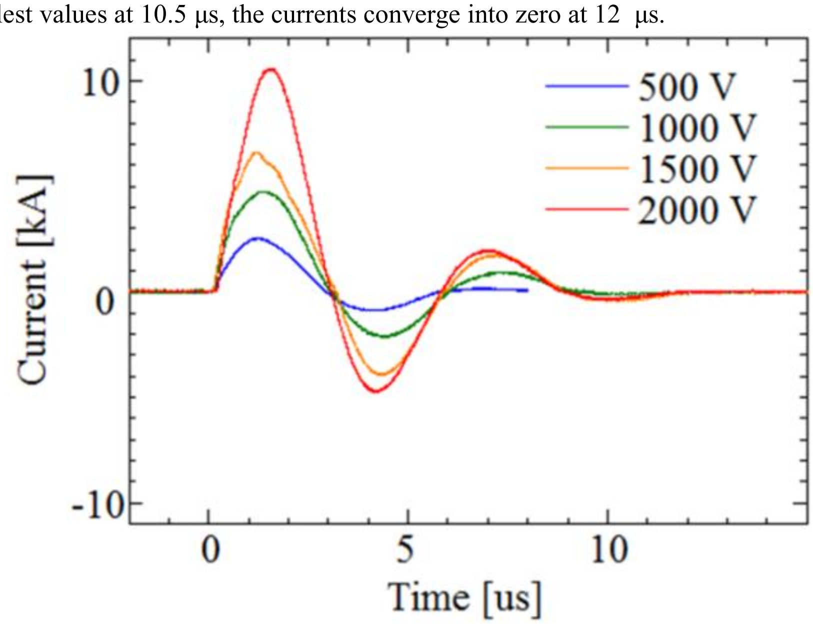

Figure 10. Discharge current waveform

B. Plasma Plume Observation with ICCD camera

ICCD images of plasma plume from a rectangular L-EM thruster are shown in Fig. 11 for V_c = 0 V, Figs. 12 and 13 for V_c = 1000 V, and Figs. 14 and 15 for V_c = 2000 V. In the figures, upper and lower electrodes are anode and cathode, respectively.

For V_c = 0 V, in Fig.11, namely for a pure laser propulsion mode, a plume starts diffusing at 0 ns. At 100-800 ns, the plume diffuses to x-direction and the emission gradually decreases and diffusing between electrodes.

For V_c = 1000 V, in Figs.12 and 13, similar behaviors of the laser propulsion mode can be seen at 0-100 ns. However, at 200 ns, different from a V_c = 0 V, a spot emission can be seen on the cathode surface. Therefore, the emission originates from discharge. At 300 ns, two planer emission structures can be seen, i.e., one near cathode and another near anode. At 400 ns, the anode side plasma precedes. At 500-1000 ns, a strong emission plume diffuses to x-direction after a sudden fall of brightness at 500 ns. At 800 ns, the plasma emission arrives at edges and strong emission can be seen at anode edge. On the other hand, after 800 ns, the planer plasmas detach from anode and extend to cathode side. At 1100-1700 ns, a sudden fall of brightness between electrode and emission can be seen at the anode edge and a cathode surface. At 1800-6000 ns, a strong luminescence can be seen near the anode and propellant surface.

For V_c = 2000 V, in Figs. 14 and 15, similar tendencies with V_c = 1000 V can be seen and a spot emission on cathode surface is observed. At 400 ns, a sudden fall of brightness is occurring. At 600-800 ns, the anode side plasma precedes and a plasma of the center of the electrodes moves to cathode. At 1000 ns, relatively strong emission can be seen in a whole electrode region. At 1500-2000 ns, strong emissions can be seen and a plasma leaks to y-direction at anode edge. Therefore, the loss of plasmas is occurring. In this case, at 800-900 ns, an edge of the plasma emission distribution arrives at electrode edge. In V_c = 1000 and 2000 V cases, the planer plasma emission was observed, extending toward anode side, which is moving faster than cathode side, at an initial pulse phase.

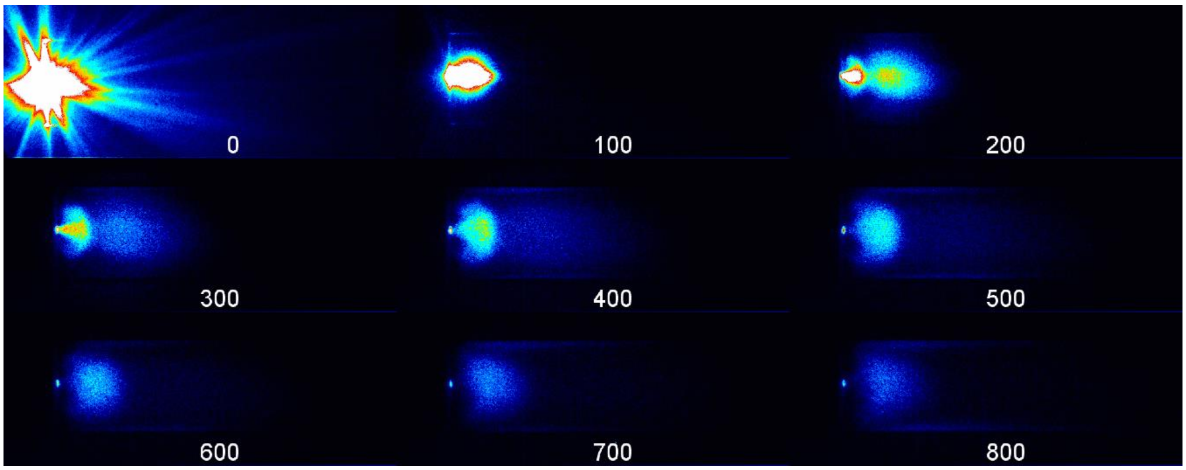

Figure 11. ICCD images of plume from a rectangular L-EM thruster (anode: higher electrode for td = 0-800 ns, *Vc* = 0 V).

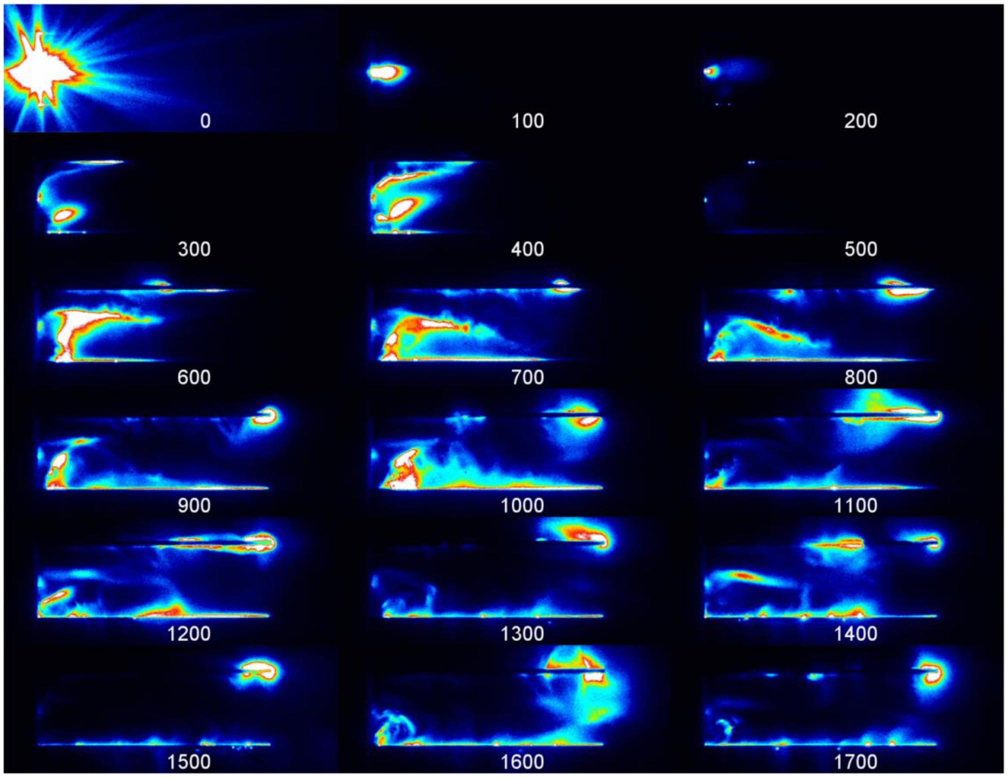

Figure 12. ICCD images of plume from a rectangular L-EM thruster (anode: higher electrode for td = 0-1700 ns, *Vc* = 1000 V).

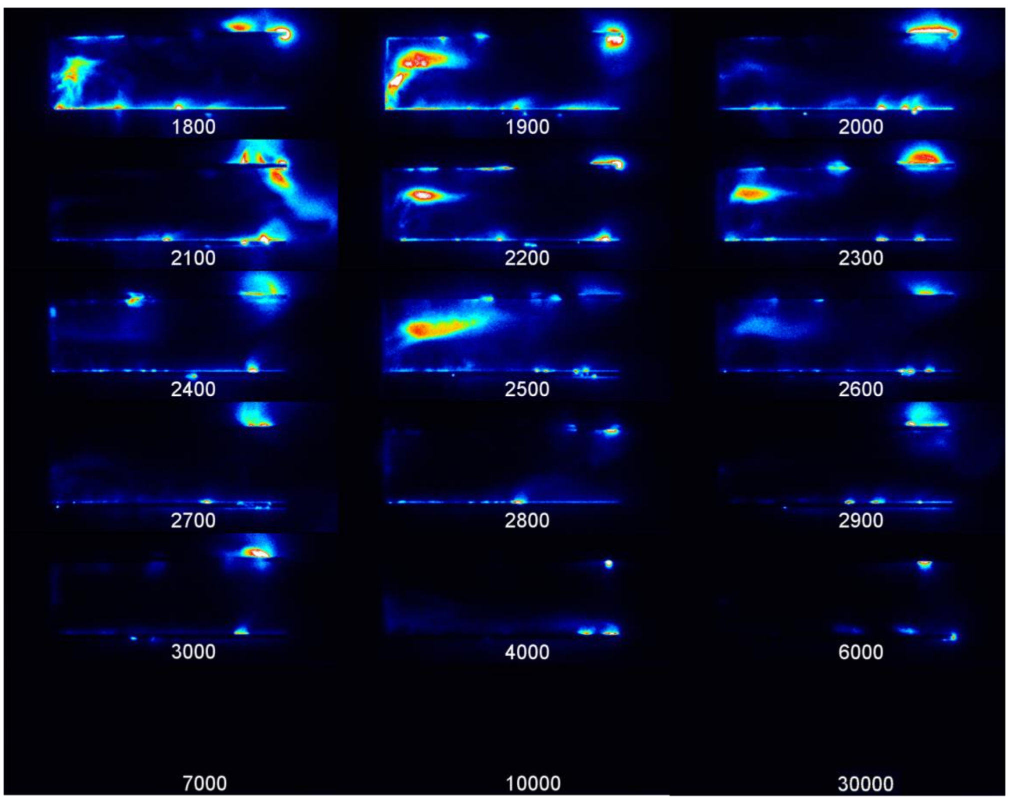

Figure 13. ICCD images of plume from a rectangular L-EM thruster (anode: higher electrode for td = 1800-30000 ns, *Vc* = 1000 V).

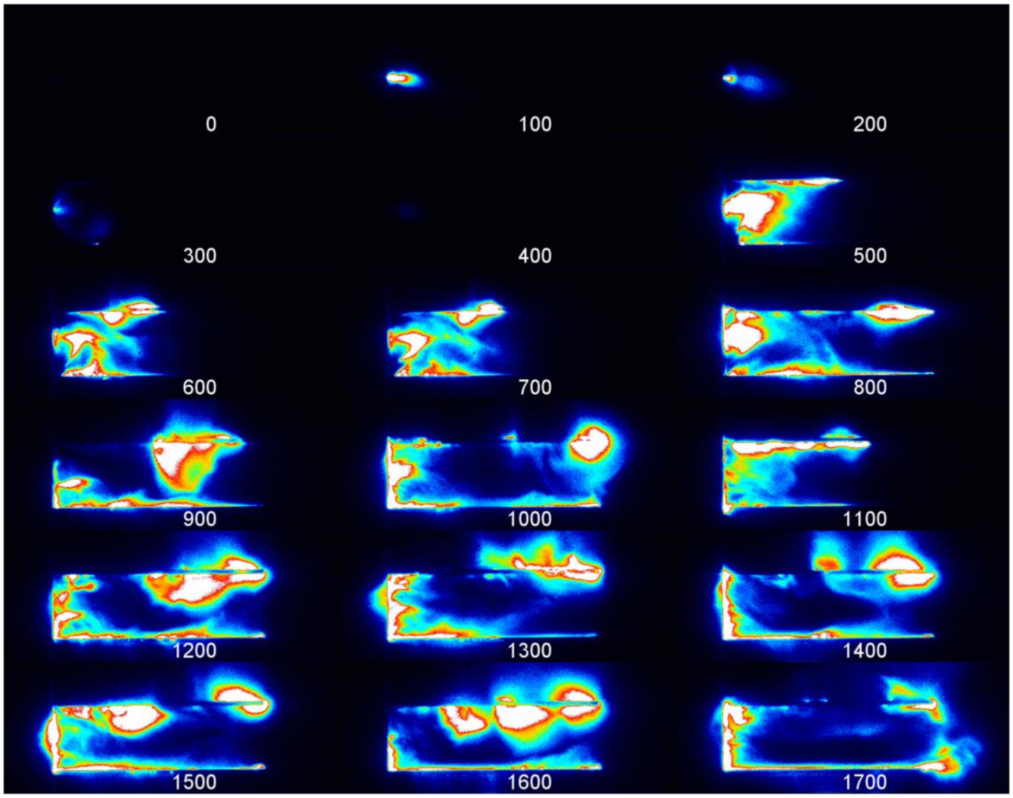

Figure 14. ICCD images of plume from a rectangular L-EM thruster (anode: higher electrode for td = 0-1700 ns, *Vc* = 2000 V).

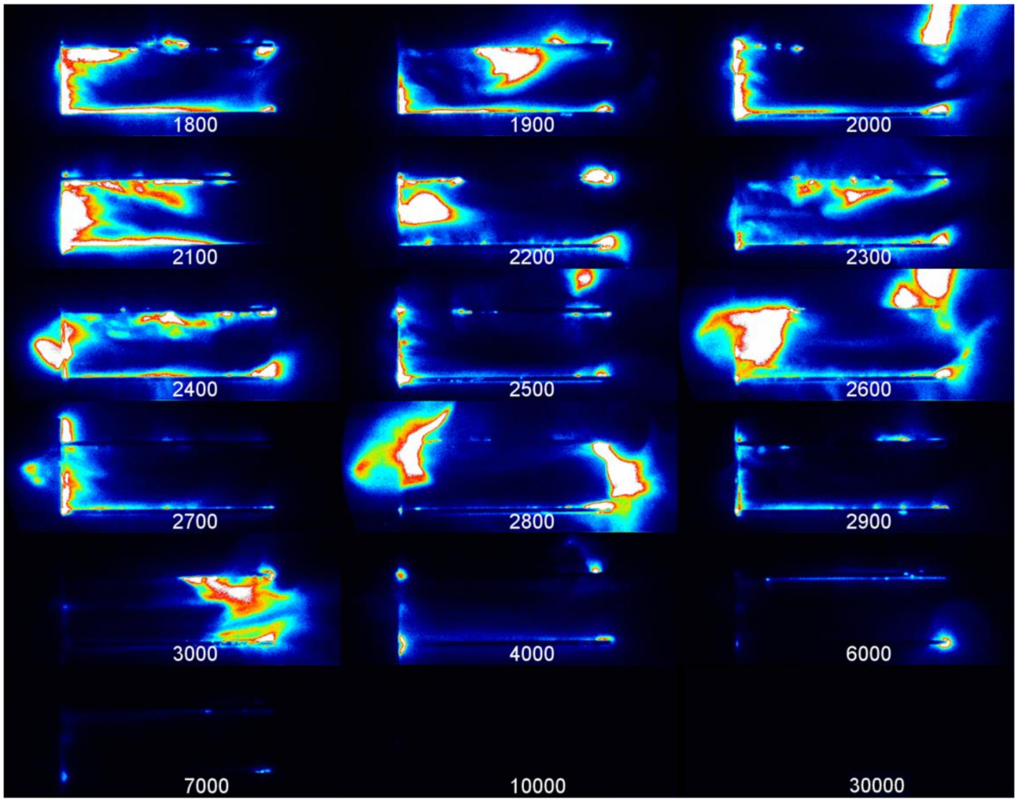

Figure 15. ICCD images of plume from a rectangular L-EM thruster (anode: higher electrode for td = 1800-30000 ns, *Vc* = 2000 V).

C. Plasma Behavior Analysis

Time-resolved images captured by the ICCD camera were analyzed with an image processing software. In the analysis, emission intensity distributions of the plasma parallel to a longitudinal direction (*x*-axis) of the thruster were plotted and evaluated from the image data, as shown in Fig. 16 (for y = 0 mm, V_c = 1000 V, measured at 900-1400 ns). As shown in the figure, a typical speed of a wavefront (an inflection point of emission distribution) of the plasma in the thruster is v_p = 55.4 km/s.

Figures 17 and 18 show the plots of time versus position of wavefront, evaluated along three lines (center line (y = 0 mm), anode side (y = 3 mm), cathode side (y = -3 mm)) parallel to a longitudinal axis (*x*-axis) of the thruster for 1000 V and 2000 V, respectively.

From the figures, it can be seen that regardless of the *y*-coordinates, the plasma wavefront is moving toward electrode edge. Larger speeds were obtained in center and anode sides than cathode side. In addition, faster motion of the wavefront of the plasma was observed in higher voltage cases. From the results, typical speeds of plasmas for V_c = 1000 V and 2000 V are 57.7 km/s and 63.1 km/s, respectively.

From the plasma speed of 63.1 km/s at V_c = 2000 V, a specific impulse estimated from the division of the speed by the gravitational acceleration (9.8 m/sec^2) gives I_{sp} = 6,400 sec On the other hand, from our previous research, specific impulse data measured from the impulse and mass shot measurements shown in Fig. 3 gives I_{sp} - 7,200 sec. This discrepancy of specific impulses estimated with the ICCD imaging is probably due to presence of some particles, i.e., neutral particles, which are still invisible with conventional ICCD camera systems.

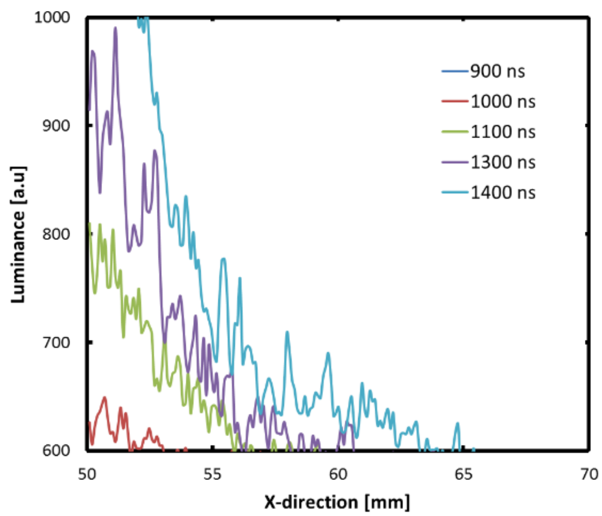

Figure 16. Examples of emission intensity distributions of the plasma parallel to x-axis of the thruster to determine speed of plasma wave front (for y = 0 mm, *Vc* =1000 V, measured at 900-1400 ns).

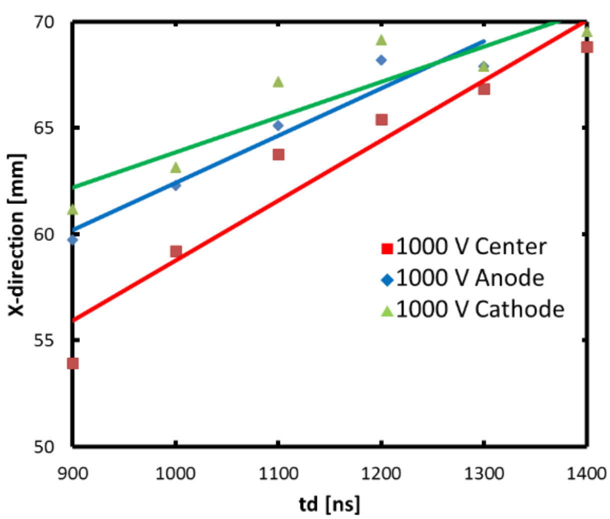

Figure 18. Motion of plasma wave front (*Vc* = 1000V).

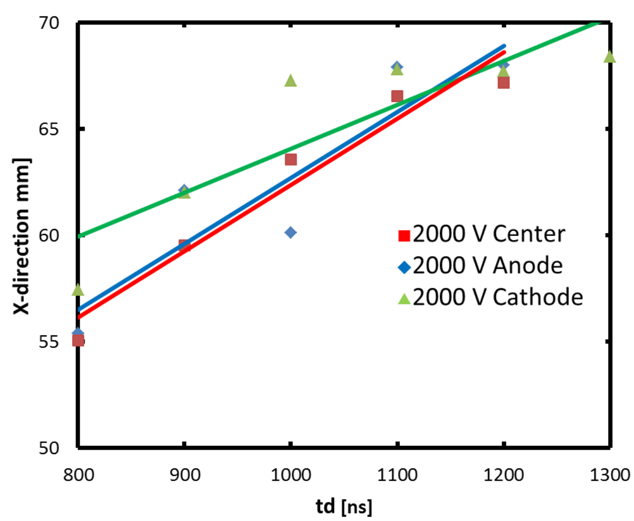

Figure 17. Motion of plasma wave front (*Vc* = 2000V).

D. Ion Emission Characteristics Measured with Faraday Cup

Typical result of temporal variations of ion current measured at 400 mm and 600 mm are shown in Fig. 19 at laser energy of 190 mJ. From the figure, it can be seen that the peak of ion current shifts toward earlier time at closer position of 400 mm. Considering times of these peaks and gap between two positions, speed of ions can also be estimated. Variations of the ion speeds with charging voltages are plotted in Fig. 20. It can be seen that ion speed velocity is increasing with charging voltages. The maximum ion speed was 220 km/s at V_c = 2000 V.

From the plasma speed of 220 km/s at V_c = 2000 V, a specific impulse estimated from the division of the speed by the gravitational acceleration (9.8 m/sec^2) gives I_{sp} = 22,400 sec.

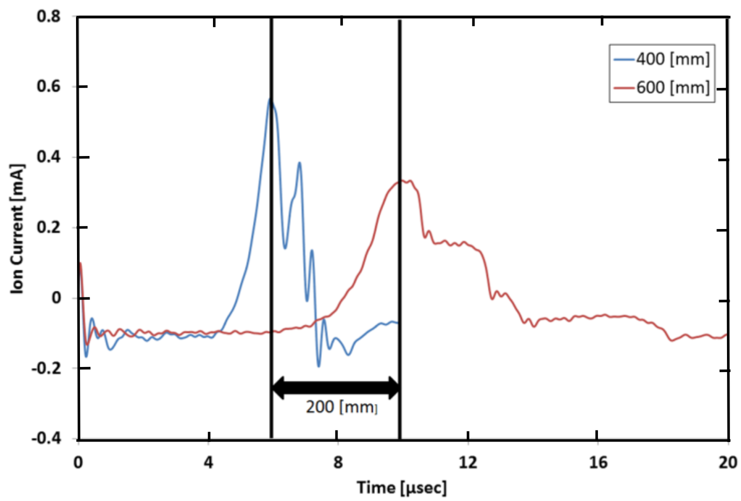

Figure 19. Schematic of comparison with distance of Faraday cup (400 mm and 600 mm).

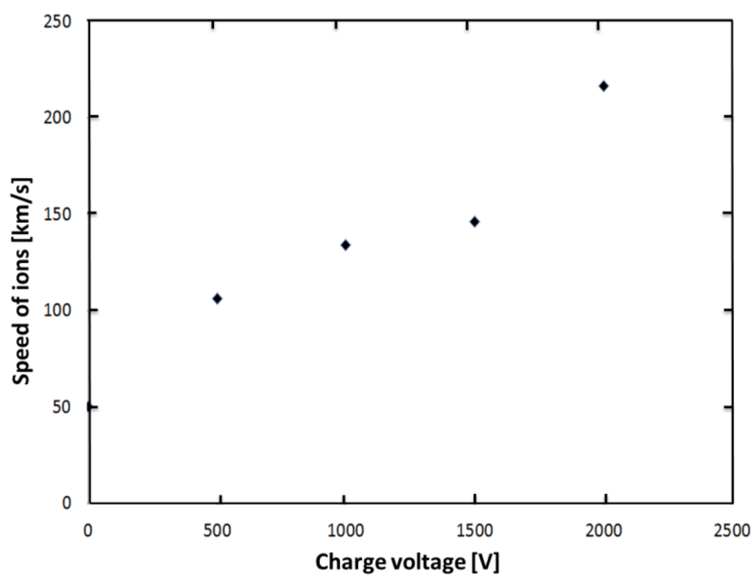

Figure 20. Ion flight velocity estimated by ion peak current.

E. Evaluation of Thrust Performance

Impulse bits and mass shot of a rectangular L-EM thruster are shown in Fig. 21. Impulse bits for E_c = 0-14.5 J (V_c =0-2000 V) were 12-85 μNs, respectively. In addition, mass shot for E_c = 0-14.5 J (V_c = 0-2000 V) were 0.8-0.9 μg per pulse, respectively. From the figure, it can be seen that impulse bit increased with charging energy. On the other hand, the mass shot is not increasing with charging energy. From these results, typical values of specific impulse and thrust efficiency were estimated. Specific impulses and thrust efficiencies for E_c=0-14.5 J (V_c = 0-2000 V) were 1,500-

9,950 sec, and η_{th} = 10-28%, respectively. From these result, a speed of plasma estimated from the division of the impulse bit by the mass shot for V_c =2000 V gives 94.4 km/s. On the other hand, specific impulse and speed of plasma estimated with the ICCD imaging for V_c =2000 V were 6,400 sec and 63.1 km/s, respectively. Furthermore, specific impulse and speed of plasma estimated with Faraday cup for V_c =2000 V were 22,400 sec and 220 km/s, respectively. This large discrepancy of specific impulses and speed of plasma estimated with the ICCD imaging were probably due to the low-luminance particles which was still invisible with conventional ICCD camera systems. In addition, large number of specific impulse is due to nature of the TOF measurement monitoring only ions.

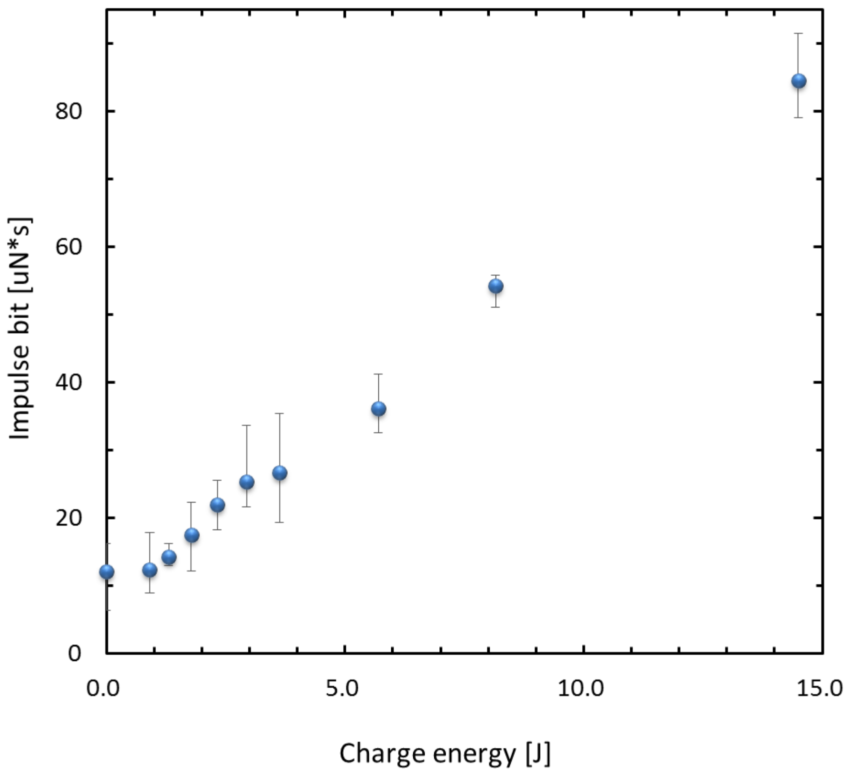

Figure 21. Impulse bit and mass shot of a rectangular L-EM thruster.

VI. Conclusions

An objective of this study was to observe the plasma acceleration process and to understand the mechanism of high speed plasma generation. To observe the plasma behaviors between the rectangular electrodes of the L-EM thruster, an ICCD camera was utilized. From the time-resolved images, behaviors of the plasma wavefront were analyzed and speeds of the plasma were estimated. Moreover, to estimate the speed of fast ions, time-of flight (TOF) measurement was conducted. In addition, to evaluate the thrust performance, impulse bit measurement and mass shot measurement were also conducted.

From the result, it can be seen that regardless of the *y*-coordinates, the plasma wavefront is moving toward electrode edge. Larger speeds were obtained in anode center side than cathode sides within V_c conditions. In addition, faster motion of the wavefront of the plasma was observed in higher voltage cases. From the results, the typical speed of plasma for V_c = 1000 V and 2000 V were 57.7 km/s and 63.1 km/s, respectively. In addition, maximum speed of plasma from result of TOF measurement was 220 km/s. Moreover, preliminary impulse bit measurement was conducted with a thrust stand. Impulse bit of rectangular L-EM thruster for V_c = 0-2000 V were 12-85 μNs. In addition, mass shot for E_c= 0-14.5 J (V_c = 0-2000 V) were 0.8-0.9 μg per pulse, respectively. Specific impulses and thrust efficiencies for E_c = 0-14.5 J (V_c = 0-2000 V) were I_{sp} = 1,500-9,950 sec and η_{th} = 10-28%, respectively. From these result, the speed of plasma estimated from the division of the impulse bit by the mass shot for V_c =2000 V gave 94.4 km/s. On the other hand, specific impulse and speed of plasma estimated with the ICCD imaging for V_c =2000 V were

6,400 sec and 63.1 km/s, respectively. Furthermore, specific impulse and speed of plasma estimated with Faraday cup for V_c =2000 V were 22,400 sec and 220 km/s, respectively.

This large discrepancy of specific impulses and speed of plasma estimated with the ICCD imaging were probably due to the low-luminance particles which was still invisible with conventional ICCD camera systems. In addition, large number of specific impulse is due to nature of the TOF measurement monitoring only ions.

References

[1]Myers, R.M., et al., "Small Satellite Propulsion Options," AIAA Paper 94-2997, June 1994.

[2]Mueller, J., "Thruster Options for Micro-spacecraft: A Review and Evaluation of Existing Hardware and Emerging Technologies," AIAA Paper 97-3058, July 1997.

[3]Leifer, S., "Overview of NASA's Advanced Propulsion Concepts Activities," AIAA Paper 98-3183, July 1998.

[4]Micci, M. M., and Ketsdever, A. D. (ed.), Micropropulsion for Small Spacecraft (Prog. Astronautics and Aeronautics 187), American Institute of Aeronautics and Astronautics, 2000.

[5]Gonzales, D., and Baker, R., "Micropropulsion using a Nd:YAG Microchip Laser," Proceedings of SPIE

[6]Pakhomov, A.V., et al., "Specific Impulse Study of Ablative Laser Propulsion," AIAA Paper 2001-3663, 2001.

[7]Horisawa, H., and Kimura I., "Fundamental Study on Laser Plasma Accelerator for Propulsion Applications," Vacuum, Vol.65 (No.3-4), pp.389-396, 2002.

[8]Horisawa, H., et al., Beamed Energy Propulsion: AIP Conference Proceedings Vol.664, 2003, pp.423-432. 10) Horisawa, H., et al., IEPC 2003-75 (2003).

[9]Kawakami, M., et al., AIAA Paper 2003-5028 (2003).

[10]Horisawa, H., et al., Applied Physics A 81, pp.303-310 (2005).

[11]Horisawa, H., et al., The Review of Laser Engineering 34, pp.435-441 (2006).

[12]Sasaki, Y., et al., IEPC 2007-56 (2007).

[13]Horisawa, H., et al, AIAA Paper 2008-4818 (2008).

[14]Ono, T., et al, AIAA Paper 2008-5008 (2008).

[15]T.E. Markusic, "Phenomenological Model of Current Sheet Canting in Pulsed Electromagnetic Accelerators", IEPC 2003-0293 p. 5-6

[16]Thomas Edward Markusic,"Current Sheet Canting in Pulsed Electromagnetic Accelerators", A DISSERTAtiON PRESENTED TO THE FACULTY OF PRINCETON June,2002p. 71

[17]Hideyuki Horisawa , "High Isp Mechanism of Rectangular Laser-Electromagnetic Hybrid Acceleration Thruster", IEPC-2011-274 p . 7-8

[18]Jahn, R. G., *Physics of Electric Propulsion*, McGraw-Hill, 1968, pp.198-316.

[19]Tony Schöenherr, et al, "Evaluation of discharge behavior of the Pulsed plasma thruster SIMP-LEX."

[20]Burton, R. L., and Turchi, P. J., "Pulsed Plasma Thruster," *Journal of Propulsion and Power*, Vol. 14, 1998, pp.716–735.